Performance Enhancement in RIS-aided Wireless Networks

Capstone Report

Torebek Toregozhin

Nazarbayev University
Department of Electrical and Computer Engineering
School of Engineering and Digital Sciences

This project report was created on TexStudio editing platform using LaTeX. All the figures were drawn using draw.io online software tool.

NAZARBAYEV UNIVERSITY

Electrical and Computer Engineering
Nazarbayev University
http://www.nu.edu.kz

Title:
Performance Enhancement in RIS-aided Wireless Networks

Theme:
Capstone Project Final Report

Project Period:
Spring 2024

Project Group:
Laboratory for Wireless Innovation

Participant(s):
Torebek Toregozhin

Supervisor(s):
Galymzhan Nauryzbayev

Copies: 1

Page Numbers: 30

Date of Completion:
April 26, 2024

Abstract:

This study explores the performance of a cooperative non-orthogonal multiple access (CNOMA) downlink wireless communication system, aided by a novel technology called simultaneously transmitting and reflecting reconfigurable intelligent surfaces (STAR-RISs), operating over Nakagami-m fading channels. The evaluation focuses on outage probability (OP), spectral efficiency (SE), and energy efficiency (EE) as key performance indicators. The mathematically intractable probability density and cumulative distribution functions of the near user are approximated using the Gamma moment-matching method. This enables the derivation of closed-form expressions for OP and ergodic rates of users, which are used to determine SE and EE. Monte-Carlo simulations validate the analytical results. A comparison with OMA and NOMA is provided to assess CNOMA's effectiveness, revealing that the cooperative link can enhance SE and EE in the STAR-RIS-based NOMA network.

Contents

Preface

I would like to express sincere gratitude to my supervisor professor Galymzhan Nauryzbayev and Mohd Hamza Naim Shaikh for all the support and guidence during this research.

Nazarbayev University, April 26, 2024

Torebek Toregozhin
<torebek.toregozhin@nu.edu.kz>

Chapter 1

Introduction

As the fifth-generation (5G) wireless systems are being implemented, academia and industry already devise candidates for the development of the future beyond-5G (B5G) and sixth-generation (6G) networks [1, 2]. Consequently, the concept of reconfigurable intelligent surfaces (RISs) has arisen as a potentially effective method for establishing intelligent and efficient radio environments [3, 4, 5].

RIS is a surface made up of multiple passive reflecting elements (RE) that can modify the amplitude and/or phase of incoming signals in a controlled manner [6, 7, 8]. However, the design of conventional reflecting-only RIS is limited to a half-space communication. To address this challenge, the notion of simultaneously transmitting and reflecting RIS (STAR-RIS) was introduced in [9].

STAR-RIS is designed, as the name suggests, to transmit and reflect incident signals at the same time, hence splitting it into two parts that “pierce through" and “bounce from" a surface of STAR-RIS. This is possible because STAR-RISs can respond to both electric and magnetic components of a signal, while conventional RISs support only electric polarization of currents. Additionally, each STAR element’s reflection and transmission coefficients can be adjusted independently, permitting non-constraint spatial flexibility of transmitted and reflected signals. In consequence, a full space 360-degree coverage can be achieved [10].

The NOMA is a multiple access technique that caught a lot of attention from researchers recently and even was considered as the strongest candidate for 5G due to its theoretical supremacy over the traditional OMA techniques in terms of user fairness, spectral efficiency (SE) and energy efficiency (EE) [11]. It is designed to support massive connectivity in densely populated user environments by utilizing the same frequency, time, and code spaces to transmit desired messages to target users. In NOMA protocol, a power imbalance is employed into superposition coding (SC) at the transmitter and successive interference cancellation (SIC) algorithms are applied at receivers to decode required messages. Such approach achieves better performance at a cost of increased complexity of receiver struc-

tures, because with SIC the receivers remove unwanted users' messages from the superimposed signal one by one in a certain sequence until the wanted message is decoded. Moreover, a residual interference due to imperfections in SIC has a considerable impact onto the quality of communication, thus, calling for the involvement of other diversity techniques to reduce decoding errors [11].

1.1 Related Works

RIS-aided Communication

The existing works prove that in the RIS-aided communication the performance of NOMA is improved as compared to traditional relaying and MA techniques. In particular, the achievable capacity of RIS-aided NOMA network was studied in [12], where the authors also made a comparison with the identical DF relay-assisted NOMA system as well as their OMA counterparts. It was shown that the NOMA systems were superior to OMA and that with a sufficient number of RE, a RIS can outperform DF relay. Further, in [13], inspired by the findings that a RIS can improve the quality of a channel to an extent, where a NOMA user in supposedly worse conditions becomes stronger than an user in supposedly better conditions, the authors demonstrated that when such conversions take place, the power allocation according to NOMA protocol should be reconsidered to avoid a decay of the achievable capacity. In [14], the authors compared the performance of RIS-aided NOMA and OMA in terms of transmit power and location of users. It was found that it is important to pair users with an asymmetric deployment in NOMA for its superiority over OMA. In [15], the authors made an insight into a RIS-aided NOMA system with non-ideal transceiver and mentioned the importance of hardware impairments consideration for a more accurate performance analysis. While in [16], the authors considered the cascaded RIS-aided networks and derived the outage probability expression for the end-to-end communication, and the authors in [17], showed that FD relay could be used to tackle the RISs' far-field propagation losses and enhance the communication between two RISs. RIS-aided multi-user multiple-input and single-output (MISO) systems were considered in [18, 19, 20], where the authors in [18] maximized EE through the optimization of power allocation and phase-shifts of RE, in [19] minimized transmit power through the joint optimization of active and passive beamforming and found that a three-fold EE improvement over multi-antenna AF relaying could be achieved, while in [20] the users' sum-rate was maximized demonstrating significant performance gains over equivalent non-RIS and OMA systems.

STAR-RIS-aided Communication

Inspired by the possibility of full-space communication, researchers started investigating STAR-RIS's performance and applications extensively. More precisely, in one of the early works on STAR-RIS, [21], the three operating protocols for STAR-RIS were proposed, namely, energy splitting (ES), mode switching (MS), and time switching (TS). According to ES, each individual STAR element can be configured to simultaneously transmit and reflect an incident signal; according to MS, each individual element is permitted only to transmit or reflect; and according to TS, all of the elements on STAR-RIS whether transmit or reflect at any given instance of time. Additionally, the authors formulated an energy consumption minimization problem for each protocol and made comparisons in unicast as well multicast downlink scenarios. Hence the advantages and disadvantages of each protocol were indicated and it was shown that STAR-RIS's energy consumption is lower than conventional RIS's, when users are located on either side of a surface. In [22], the algorithms for an energy efficient STAR-RIS-aided multiple input multiple output (MIMO)-NOMA communication system with multiple user pairs were proposed. The simulation results demonstrated the performance superiority of NOMA over OMA schemes. The transmit power minimization for the uplink communication was studied in [23]. In addition, the achievable rate performance of STAR-RIS-aided massive MIMO network was presented by the authors in [24].The analysis included imperfect channel estimation, spatial channel correlation, and operation of STAR-RIS under three protocols discussed earlier in this section. In [25], the authors provided performance analysis of the STAR-RIS-aided communication systems in terms of outage probability (OP), achievable rates, and symbol error rate (SER) and found out that asymptotically the achievable rates and SER depend on the power allocation rather than the operation protocol and resource allocation on a STAR-RIS. The more in-depth performance analysis of STAR-RIS-aided system was provided in [26], where, additionally, the effect of imperfect SIC was considered. As a result, it was shown that the OP of STAR-RIS-NOMA outperforms its OMA counterpart as well as conventional cooperative communication techniques such as DF and AF relaying. In [27], the authors made the ergodic rate analysis with statistical channel state information (CSI) and proposed the suboptimal STAR-RIS phase-shift scheme. In [28], the authors investigate the performance of STAR-RIS-aided overlay cognitive radio NOMA in the industrial setup in terms of OP, ergodic rates and EE. They demonstrated that by increasing the number of STAR-RIS elements the system's reliability and EE can be enhanced, especially in comparison with OMA as NOMA protocol allows to allocate several users to share the same resource blocks. Further, the joint reliability and beamforming optimization of STAR-RIS-assisted multiple input single output system, also in the industrial IoT scenario, was covered by the authors in [29]. They proposed adaptable deep reinforcement learning algorithm for the real time changes, while con-

sidering channel estimation errors. In [30], the authors proposed a meta-learning approach for the joint optimization of multi-STAR-RIS-aided FD systems. Moreover, they made the comparison with equivalent multi-RIS-aided system, showing that STAR-RIS-aided systems can achieve higher sum-rates. In [31], the authors proposed resource allocation algorithms for STAR-RIS-aided NOMA and OMA systems. The numerical results illustrate that STAR-RIS-aided NOMA significantly outperforms conventional RIS and OMA networks. The coupled phase-shift STAR-RIS model was proposed in [32]. Then in [33], the extension of the previous work, with more in-depth explanation of the proposed hardware model, the authors propose three practical phase-shift configuration strategies. The combination of STAR-RIS-NOMA for integrated sensing and communication was considered in [34], where they proposed suboptimal solution of the non-convex joint power allocation, active and passive beamforming optimization problem. The full-duplex STAR-RIS-aided system with the downllink and uplink users is studied in [35]. The authors showed that STAR-RIS can provide approximately 5%-50% better performance in terms of OP and throughput. The dual-sided incidence of STAR-RISs was studied in [36], where the performance of STAR-RIS-aided system with two uplink users was analysed for NOMA and OMA. And the indoor and outdoor 3D localization performance limits of STAR-RIS were studied in [37].

1.2 Motivation

Despite the relative novelty of the topic it is obvious that the STAR-RIS-aided NOMA communication was already studied in literature, however, the performance of STAR-RIS-aided cooperative NOMA (CNOMA) systems was not fully investigated yet. Moreover, other works on RIS-aided CNOMA, [38, 39, 40, 41, 42, 43], suggest an improvement in performance over non-cooperative NOMA. Thus, the objective of this work is to see if it is possible to enhance performance of STAR-RIS-aided NOMA systems by introducing additional cooperative phase into the downlink transmission and draw some meaningful insignts about the system.

Chapter 2

System Model

2.1 Network Model

As illustrated in Fig. 2.1, the STAR-RIS-aided CNOMA downlink communication system, wherein BS attempts to communicate with a set of multiple users is considered. Each user is sorted into a subset of users served by a separate beam based on the location. Beamforming is performed to suppress the interference between the subsets, while SIC is performed to mitigate the inter-user interference within each subset [44].

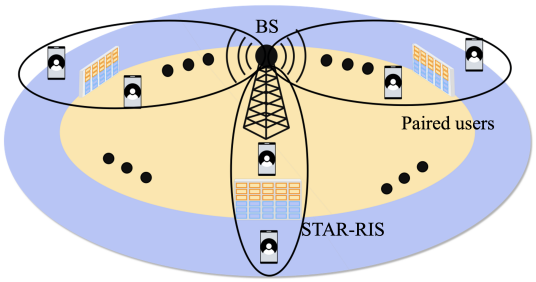

Figure 2.1: STAR-RIS-empowered NOMA communication, generalized schematic.

Due to supposed similarities between the subsets, this study is concerned with the analysis of a single representative cluster[1] with two users[2] as in Fig. 2.2, where NU is located at the cell center, FU is located at the cell edge, and STAR-RIS is located between them to strengthen the channel gains. According to the assumptions of previous studies [45], FU is outside of the BS's direct coverage region because

[1]Although the results are derived only for one such representative cluster, they can easily be extended for a set of clusters in a STAR-RIS-aided NOMA network. However, the joint clustering and optimization would be out of scope for this work and will be considered for future work.

[2]This system model is limited to two paired users due to propagation error and complexity restrictions as in [21, 22, 25, 26, 27, 31, 32, 33, 35, 36, 37].

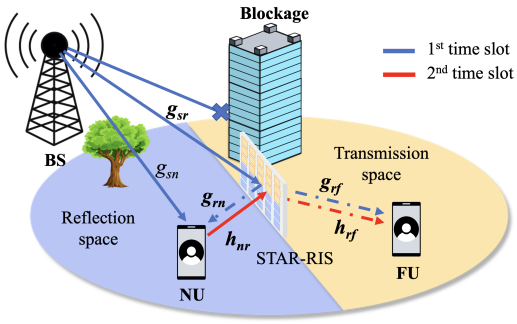

Figure 2.2: STAR-RIS-empowered NOMA communication within each cluster. Here, the solid lines represent the direct link from the base station, while the dashed lines represent the reflected/transmitted links.

of environmental factors such as blockages or distance, and, in contrast, NU has access to a direct link with BS. Therefore, FU accesses the communication via a STAR-RIS-aided link.

It is assumed that STAR-RIS operates under the MS protocol and has M number of elements, where M_r elements operate in the reflection mode. The remaining M_t elements operate in the transmission mode, and $M_r + M_t = M$. Subsequently, the STAR-RIS's reflection and transmission coefficient matrices are denoted as $\mathbf{\Theta}_r = \text{diag}\left(\sqrt{\beta_{r,1}}e^{j\theta_{r,1}}, \sqrt{\beta_{r,2}}e^{j\theta_{r,2}}, \cdots, \sqrt{\beta_{r,M}}e^{j\theta_{r,M}}\right)$ and $\mathbf{\Theta}_t = \text{diag}(\sqrt{\beta_{t,1}}e^{j\theta_{t,1}}, \sqrt{\beta_{t,2}}e^{j\theta_{t,2}}, \cdots, \sqrt{\beta_{t,M}}e^{j\theta_{t,M}})$, respectively, where $\sqrt{\beta_{r,i}}$ and $\sqrt{\beta_{t,i}}$ represent the amplitude response, and $\theta_{r,i}$ and $\theta_{t,i}$ represent the phase shift of the i-th element, i.e $\beta_{r,i}, \beta_{t,i} \in \{0,1\}$, and $\theta_{r,i}, \theta_{t,i} \in [0, 2\pi)$, $\forall\, i = \{1, \cdots, M\}$. Additionally, the amplitude response is constrained by the law of conservation of energy as follows: $\beta_{r,i} + \beta_{r,i} = 1$.

2.2 Cooperative NOMA Protocol

To enable cooperative communication, the downlink transmission occurs in two timeslots. During the first timeslot (FTS), according to the NOMA protocol, BS applies SC to transmit the symbol x to the paired users, NU and FU, as follows

$$x = \alpha_n\, x_n + \alpha_f\, x_f, \tag{2.1}$$

where x_n and x_f denote the symbols intended for NU and FU, α_n and α_f denote the power allocation coefficients for NU and FU, respectively, which follow the principles of power domain NOMA, i.e., $\alpha_n^2 + \alpha_f^2 = 1$. Due to the larger distance of FU from BS, we use $\alpha_n < \alpha_f$. Then, NU applies SIC to decode FU's message to subtract it from the received superimposed signal and obtain its own message.

During the second timeslot (STS), to enhance the quality of communication at FU, NU utilizes the information about the FU's message acquired in FTS, x_f', and re-transmits it to FU. For the duration of STS, BS transmits neither to NU nor

FU. At the same time, FU uses maximum ratio combining to combine the signals received from both timeslots.

2.3 Channel Model

To distinguish the fading channel coefficients in FTS and STS, the lowercase letters "g" and "h" are used, respectively. Double subscripts are added to indicate a link, where the first letter refers to a transmitting node and the second letter refers to a receiving node of the link. Thus, to indicate BS, STAR-RIS, NU, and FU, the lowercase letters s, r, n, and f are used, respectively. Additionally, it is assumed that all channels are quasi-static, flat fading, and the perfect CSI is available at BS.

Thus, the BS-to-STAR-RIS link is denoted as $\mathbf{g}_{sr} = [g_{sr}^{(1)}, \ldots, g_{sr}^{(n)}, \ldots, g_{sr}^{(M)}]$, where $g_{sr}^{(i)} \sim \mathcal{NK}\left(m_{g_{sr}}, \Omega_{g_{sr}}\right)$, $\forall i$, which denotes a Nakagami-m random variable (RV) with the shape parameter $m_{g_{sr}}$ and spread parameter $\Omega_{g_{sr}}$. The BS-to-NU link is denoted as g_{sn} and $\mathrm{g}_{sn} \sim \mathcal{NK}\left(m_{g_{sn}}, \Omega_{g_{sn}}\right)$. The STAR-RIS-to-NU link is denoted as $\mathbf{g}_{rn} = [g_{rn}^{(1)}, \ldots, g_{rn}^{(n)}, \ldots, g_{rn}^{(M)}]^H$, where $g_{rn}^{(i)} \sim \mathcal{NK}\left(m_{g_{rn}}, \Omega_{g_{rn}}\right)$, $\forall i$. The STAR-RIS-to-FU link in FTS is denoted as $\mathbf{g}_{rf} = [g_{rf}^{(1)}, \ldots, g_{rf}^{(n)}, \ldots, g_{rf}^{(M)}]^H$, where $g_{rf}^{(i)} \sim \mathcal{NK}\left(m_{g_{rf}}, \Omega_{g_{rf}}\right)$, $\forall i$. The NU-to-STAR-RIS link is denoted as $\mathbf{h}_{nr} = [h_{nr}^{(1)}, \ldots, h_{nr}^{(n)}, \ldots, h_{nr}^{(M)}]$, where $h_{nr}^{(i)} \sim \mathcal{NK}\left(m_{h_{nr}}, \Omega_{h_{nr}}\right)$, $\forall i$. Finally, the STAR-RIS-to-FU link in STS is denoted as $\mathbf{h}_{rf} = [h_{rf}^{(1)}, \ldots, h_{rf}^{(n)}, \ldots, h_{rf}^{(M)}]^H$, where $h_{rf}^{(i)} \sim \mathcal{NK}\left(m_{h_{rf}}, \Omega_{h_{rf}}\right)$, $\forall i$. Additionally, the shape parameter $m = 1$ for a given Nakagami-m fading channel denotes the non-line-of-sight (NLoS), and $m > 1$ correspondingly denotes the line-of-sight (LoS) propagation scenarios.

While the distance-dependent path loss is characterized using the 3GPP Urban Micro path loss model described in [46], the path loss Λ at the carrier frequency of 3 GHz and a distance of d meters can be expressed as

$$\begin{aligned}\Lambda(d)\ [\mathrm{dB}] = G_{\mathrm{t}}\ [\mathrm{dBi}] + G_{\mathrm{r}}\ [\mathrm{dBi}] \\ + \begin{cases} -37.5 - 22\log_{10}(d/1\,\mathrm{m}) & \text{if LoS,} \\ -35.1 - 36.7\log_{10}(d/1\,\mathrm{m}) & \text{if NLoS,} \end{cases}\end{aligned} \tag{2.2}$$

where G_{t} and G_{r} denote the transmit and receive antenna gains at the transmitting and receiving nodes, respectively.

2.3.1 Received Signal Model

First Timeslot

As follows from the cooperative NOMA protocol mentioned earlier, the received signal at NU (y_n) in FTS can be defined as

$$y_n = \left(\sqrt{\Lambda_{sn}}\, g_{sn} + \sqrt{\Lambda_{sr}\,\Lambda_{rn}}\, \mathbf{g}_{sr}\boldsymbol{\Theta}_r\mathbf{g}_{rn}\right) \times \left(\alpha_n\, x_n + \alpha_f\, x_f\right)\, \sqrt{P_t} + w_o, \tag{2.3}$$

where P_t and w_o denote the transmit power at BS and the additive white Gaussian noise (AWGN), with $w_o \sim \mathcal{CN}(0, \sigma^2)$, respectively. Λ_{sn}, Λ_{sr} and Λ_{rn} denote the path loss for the BS-to-STAR-RIS and STAR-RIS-to-NU links.

Similarly, the received signal at FU (y_{f1}) in FTS can be defined as

$$y_{f1} = \left(\sqrt{\Lambda_{sr}\,\Lambda_{rf}}\, \mathbf{g}_{sr}\boldsymbol{\Theta}_{t1}\mathbf{g}_{rf}\right) \times \left(\alpha_n\, x_n + \alpha_f\, x_f\right)\, \sqrt{P_t} + w_o, \tag{2.4}$$

where $\boldsymbol{\Theta}_{t1}$ and Λ_{rf} denote the FTS transmission coefficient matrix and path loss for the STAR-RIS-to-FU link, respectively.

Through suitable adjustment of $\theta_{r,i}$ and $\theta_{t1,i}$, the received signal power at the users can be maximized, i.e., $|\mathbf{g}_{sr}\boldsymbol{\Theta}_r\mathbf{g}_{rn}| = \left|\sum_{i=1}^{M_r} g_{sr}^{(i)}\sqrt{\beta_{r,i}}e^{j\theta_{r,i}}\, g_{rn}^{(i)}\right|$ and $\left|\mathbf{g}_{sr}\boldsymbol{\Theta}_{t1}\mathbf{g}_{rf}\right| = \left|\sum_{i=1}^{M_t} g_{sr}^{(i)}\sqrt{\beta_{t,i}}e^{j\theta_{t1,i}}g_{rf}^{(i)}\right|$ are maximized, where $g_{sr}^{(i)}$, $g_{rn}^{(i)}$, and $g_{rf}^{(i)}$ are the i-th elements of $\mathbf{g}_{sr}$, $\mathbf{g}_{rn}$, and $\mathbf{g}_{rf}$, respectively. Assuming STAR-RIS to be lossless, the maximum achievable channel gain at NU during FTS is given by

$$\begin{aligned}|\mathcal{G}_n|^2 &= \left|\sqrt{\Lambda_{sn}}\, \mathrm{g} + \sqrt{\Lambda_{sr}\,\Lambda_{rn}}\, \mathbf{g}_{sr}\boldsymbol{\Theta}_r\mathbf{g}_{rn}\right|^2 \\ &= \left(\sqrt{\Lambda_{sn}}\, |g| + \sqrt{\Lambda_{sr}\,\Lambda_{rn}} \sum_{i=1}^{M_r} \left|g_{sr}^{(i)}\right| \left|g_{rn}^{(i)}\right|\right)^2.\end{aligned} \tag{2.5}$$

Accordingly, the maximum achievable channel gain at FU during FTS is given by

$$\begin{aligned}\left|\mathcal{G}_{f1}\right|^2 &= \left|\sqrt{\Lambda_{sr}\,\Lambda_{rf}}\, \mathbf{g}_{sr}\boldsymbol{\Theta}_{t1}\mathbf{g}_{rf}\right|^2 \\ &= \left(\sqrt{\Lambda_{sr}\,\Lambda_{rf}} \sum_{i=1}^{M_t} \left|g_{sr}^{(i)}\right| \left|g_{rf}^{(i)}\right|\right)^2.\end{aligned} \tag{2.6}$$

As a result, SINR at NU can be expressed as

$$SINR_{n\to f} = \frac{|\mathcal{G}_n|^2\, \alpha_f^2\, P_t}{|\mathcal{G}_n|^2\, \alpha_n^2\, P_t + \sigma^2} = \frac{|\mathcal{G}_n|^2\, \alpha_f^2\, \gamma_t}{|\mathcal{G}_n|^2\, \alpha_n^2\, \gamma_t + 1}, \tag{2.7}$$

where $\gamma_t = P_t/\sigma^2$ is the transmit SNR at BS. Then, after excluding the interference, NU decodes its signal using SNR given by

$$SNR_n = \alpha_n^2 \ |\mathcal{G}_n|^2 \ \gamma_t. \tag{2.8}$$

Likewise, FU decodes its signal, considering NU's signal for interference. Hence, its SINR can be defined as

$$SINR_{f1} = \frac{\left|\mathcal{G}_{f1}\right|^2 \alpha_f^2 \, \gamma_t}{\left|\mathcal{G}_{f1}\right|^2 \alpha_n^2 \, \gamma_t + 1}. \tag{2.9}$$

Second Timeslot

NU re-transmits FU's signal, x'_f, decoded during FTS. Thus, the received signal by FU in STS can be defined as

$$y_{f2} = \left(\sqrt{\Lambda_{nr}\,\Lambda_{rf}}\,\mathbf{h}_{nr}\,\mathbf{\Theta}_{t2}\,\mathbf{h}_{rf}\right)\ x'_f\,\sqrt{P_n} + w_o, \tag{2.10}$$

where $\mathbf{\Theta}_{t2}$, P_t, P_n and w_o denote the STS transmission coefficient matrix, transmit power at BS, transmit power at NU, and the additive white Gaussian noise (AWGN), with $w_o \sim \mathcal{CN}(0, \sigma^2)$, respectively.

Similar to FTS, through suitable adjustment of $\theta_{t2}^{(i)}$, the received signal power at FU can be maximized, i.e., $\left|\mathbf{h}_{nr}\mathbf{\Theta}_{t2}\mathbf{h}_{rf}\right| = \left|\sum_{i=1}^{M} h_{nr}^{(i)}\sqrt{\beta_{t,i}}e^{j\theta_{t2,i}}h_{rf}^{(i)}\right|$ are maximized, where $h_{nr}^{(i)}$, and $h_{rf}^{(i)}$ are the i-th elements of $\mathbf{h}_{nr}$ and $\mathbf{h}_{rf}$, respectively. The maximum achievable channel gain at FU during STS is given by

$$\begin{aligned}\left|\mathcal{G}_{f2}\right|^2 &= \left|\sqrt{\Lambda_{nr}\,\Lambda_{rf}}\,\mathbf{h}_{nr}\mathbf{\Theta}_{t2}\mathbf{h}_{rf}\right|^2 \\ &= \left(\sqrt{\Lambda_{nr}\,\Lambda_{rf}}\,\sum_{i=1}^{N}\left|h_{nr}^{(i)}\right|\left|h_{rf}^{(i)}\right|\right)^2.\end{aligned} \tag{2.11}$$

As FU receives the signal in the presence of AWGN, the received SNR can be formulated as

$$SNR_{f2} = \left|\mathcal{G}_{f2}\right|^2 \ \gamma_n, \tag{2.12}$$

where $\gamma_n = P_n/\sigma^2$ is the transmit SNR at NU.

Chapter 3

Methodology

The initial stage of the project involved extensive exploration and thorough examination of the existing works pertaining to RIS- and STAR-RIS-aided wireless communication networks. It was primarily done to identify the research gap in the existing literature and lay the foundation for a design of the RIS-aided communication system with enhanced performance deacribed in the previous chapter.

3.1 Development of System Model

Once the communication system was decided, it was comprehensively described using the generally accepted mathematical models of received signals, flat-fading channels, STAR-RIS's transmission and reflection matrices, and etc.

3.2 Performance Evaluation Metrics

Widely accepted key performance metrics such as OP, SE and EE were chosen to analyse the designed communication system. OP is used to evaluate the system's reliability, as it shows the probablity of information rate falling below a certain threshold [47]. Similarly, SE and EE are important performance metrics that help to assess how well the spectrum and energy resources are utilized. Additionally, SE and EE are considered as the target performance metrics for the future communication networks [48].

3.2.1 Derivation of theoretical expressions

The derivation of the closed-form expressions of OP, SE and EE involved the use of widely accepted mathematical notions and approximation techniques. In addition, the definitions of chosen performance metrics were explicitly stated and facilitated by corresponding mathematical formulations.

3.2.2 Simulations

Correctness of the derived analytical expressions were validated through extensive Monte Carlo simulations in MATLAB. The simulations were parameterized in a way to match the real world values as much as possible.

Chapter 4

Results and Discussions

4.1 Analytical Expressions

Some of the operators' and functions' notations that were used during the derivation of the closed-form expressions are listed in Table 4.1.

Table 4.1: Notations

Symbol	Definition
$\mathbb{E}[\cdot]$	Expectation Operator
$\mathbb{P}[\cdot]$	Probability
$\mathbb{V}[\cdot]$	Variance Operator
$[\cdot]^{\mathrm{H}}$	Conjugate Transpose Operator
$\lvert\cdot\rvert$	Absolute Value Operator
$\Gamma(\cdot)$	Gamma Function
$\psi^{(v)}(\cdot)$	Polygamma Function of v order
$\gamma(\cdot,\cdot)$	Lower Incomplete Gamma Function
${}_pF_q(\cdot,\cdot;\cdot;\cdot)$	Generalized Hyper-Geometric Function
$f_{\mathcal{G}}(x)$, $F_{\mathcal{G}}(x)$	PDF and CDF of RV $\mathcal{G}$

4.1.1 Preliminary on Gamma Moment-Matching Technique

Since the exact probability density function (PDF) of $|\mathcal{G}_n|$ is mathematically intractable, it is approximated through the Gamma moment-matching technique.

Lemma 1. *The PDF and cumulative distribution function (CDF) of $|\mathcal{G}_n|$ obtained through the Gamma moment-matching technique can be defined as*

$$f_{|\mathcal{G}_n|}(x) = \frac{\beta^{\alpha}\, x^{\alpha-1}\, \exp(-\beta\, x)}{\Gamma(\alpha)} \text{ and} \tag{4.1}$$

$$F_{|\mathcal{G}_n|}(x) = \frac{\gamma(\alpha, \beta\, x)}{\Gamma(\alpha)}, \tag{4.2}$$

respectively, where α and β are the parameters of the Gamma distribution defined as $\alpha = \frac{\mathbb{E}[|\mathcal{G}_n|]^2}{\mathbb{V}[|\mathcal{G}_n|]}$ and $\beta = \frac{\mathbb{E}[|\mathcal{G}_n|]}{\mathbb{V}[|\mathcal{G}_n|]}$

Proof. The proof can be viewed in Appendix A.1. ■

4.1.2 Outage Probability

OP is defined as the probability of receiving SNR or SINR falling below a predefined threshold SNR, γ_k^{th}, that is related to the target data rate, R_k^{th}, through $\gamma_k^{th} = 2^{R_k^{th}} - 1$, where $k \in \{n, f1, f2\}$ indicates the user and timeslot.

First Timeslot

Since NU at first receives a superimposed signal and then applies SIC to remove the interference, the general OP can be defined as

$$P_{out,n} = \mathbb{P}\{SINR_{n\to f} \leq \gamma_f^{th}\} + \mathbb{P}\{SINR_{n\to f} > \gamma_f^{th}\} \times \mathbb{P}\{SNR_n \leq \gamma_n^{th}\}. \tag{4.3}$$

Lemma 2. *The closed-form OP expression for NU in FTS can be defined as*

$$P_{out,n} = \frac{\gamma(\alpha, \beta\Psi_{max})}{\Gamma(\alpha)}, \tag{4.4}$$

where $\Psi_{max} = \max(\Psi_1, \Psi_2) \geq 0$, with $\Psi_1 = \sqrt{\frac{\gamma_n^{th}}{\alpha_n^2\gamma_t - \alpha_f^2\gamma_t\gamma_n^{th}}}$ and $\Psi_2 = \sqrt{\frac{\gamma_n^{th}}{\alpha_n^2\gamma_t}}$.

Proof. The general OP expression from (4.3) can be re-written in terms of $|\mathcal{G}_n|$ as follows

$$P_{out,n} = \mathbb{P}\{|\mathcal{G}_n| \leq \Psi_1\} + \mathbb{P}\{|\mathcal{G}_n| > \Psi_1\} \times \mathbb{P}\{|\mathcal{G}_n| \leq \Psi_2\},$$

which can be further modified as

$$P_{out,n} = \mathbb{P}\{|\mathcal{G}_n| \leq \Psi_1\} + \mathbb{P}\{\Psi_1 < |\mathcal{G}_n| \leq \Psi_{max}\}. \tag{4.5}$$

Since the probability terms in (4.5) are mutually exclusive, it can be simplified to

$$P_{out,n} = 1 - \mathbb{P}\{|\mathcal{G}_n| > \Psi_{max}\} = F_{|\mathcal{G}_n|}(\Psi_{max}), \tag{4.6}$$

where $F_{|\mathcal{G}_n|}(\cdot)$ is the CDF of $|\mathcal{G}_n|$. Thus, by substituting (4.2) into (4.6), the expression in (4.4) is found.

This concludes the proof of Lemma 2. ■

Following the definition mentioned earlier, the general OP expression of FU can be defined as

$$P_{out,f1} = \mathbb{P}\{SINR_{f1} \leq \gamma_{f1}^{th}\} \tag{4.7}$$

Lemma 3. *The closed-form OP expression for FU in FTS can be defined as*

$$P_{out,f1} = \frac{\gamma(a_1+1, \frac{\sqrt{\Psi_3}}{b_1})}{\Gamma(a_1+1)}, \tag{4.8}$$

where $\Psi_3 = \frac{\gamma_{f1}^{th}}{(\alpha_f^2 - \gamma_{f1}^{th}\alpha_n^2)\gamma_t} \geq 0$.

Proof. After simple algebraic manipulations, the equation in (4.7) can be re-written in terms of $|\mathcal{G}_{f1}|^2$ as follows

$$P_{out,f1} = \mathbb{P}\{|\mathcal{G}_{f1}|^2 \leq \Psi_3\} = F_{|\mathcal{G}_{f1}|^2}(\Psi_3), \tag{4.9}$$

where $F_{|\mathcal{G}_{f1}|^2}(\cdot)$ represents the CDF of $|\mathcal{G}_{f1}|^2$.

Similar to [49], the PDF and CDF can be defined as

$$f_{|\mathcal{G}_{f1}|^2}(x) = \frac{x^{\frac{a-1}{2}}}{2b_1^{a_1+1}\Gamma(a_1+1)} \exp\left(-\frac{\sqrt{x}}{b_1}\right) \quad \text{and} \tag{4.10}$$

$$F_{|\mathcal{G}_{f1}|^2}(x) = \frac{\gamma\left(a_1+1, \frac{\sqrt{x}}{b}\right)}{\Gamma\left(a_1+1\right)}, \tag{4.11}$$

where the constant parameters a_1 and b_1 are defined as:

$$a_1 = \frac{(M_r+1)k_3^2k_4^2 - k_1k_5k_2k_6}{k_1k_5k_2k_6 - k_3^2k_4^2} \text{ and} \tag{4.12}$$

$$b_1 = \frac{k_5k_2k_6 - k_3^2k_4^2}{\sqrt{\frac{m_{gsr}}{\Omega_{gsr}}}k_1k_3\sqrt{\frac{m_{g_{rf}}}{\Omega_{g_{rf}}}}k_2k_4}, \tag{4.13}$$

where $k_1 = \Gamma(m_{g_{sr}})$, $k_2 = \Gamma(m_{g_{rf}})$, $k_3 = \Gamma(m_{g_{sr}} + \frac{1}{2})$, $k_4 = \Gamma(m_{g_{rf}} + \frac{1}{2})$, $k_5 = \Gamma(m_{g_{sr}} + 1)$, and $k_6 = \Gamma(m_{g_{rf}} + 1)$. Hence, the expression in (4.8) can be obtained by substituting (4.11) into (4.9).

This concludes the proof of Lemma 3. ■

Second Timeslot

Similar to FTS, the general OP expression for FU in STS can be defined as

$$P_{out,f2} = \mathbb{P}\{SNR_f \leq \gamma_{f2}^{th}\}. \tag{4.14}$$

Lemma 4. *The closed-form OP expression for FU in STS can be defined as*

$$P_{out,f2} = \frac{\gamma(a_2+1, \frac{\sqrt{\Psi_4}}{b_2})}{\Gamma(a_2+1)}, \tag{4.15}$$

where $\Psi_4 = \frac{\gamma_{f2}^{th}}{\gamma_n} \geq 0$.

Proof. Similar to the proof of Lemma 3, one can show that

$$P_{out,f2} = F_{|\mathcal{G}_{f2}|^2}(\Psi_4). \tag{4.16}$$

The PDF and CDF can be defined in a similar way as (4.10) and (4.11) were defined in the proof of Lemma 3:

$$f_{|\mathcal{G}_{f2}|^2}(x) = \frac{x^{\frac{a_2-1}{2}}}{2b_2^{a_2+1}\Gamma(a_2+1)} \exp\left(-\frac{\sqrt{x}}{b_2}\right) \text{ and} \tag{4.17}$$

$$F_{|\mathcal{G}_{f2}|^2}(x) = \frac{\gamma\left(a_2+1, \frac{\sqrt{x}}{b_2}\right)}{\Gamma\left(a_2+1\right)}, \tag{4.18}$$

where the constant parameters a_2 and b_2 are defined as:

$$a_2 = \frac{(M+1)q_3^2q_4^2 - q_1q_5q_2q_6}{q_1q_5q_2q_6 - q_3^2q_4^2} \text{ and} \tag{4.19}$$

$$b_2 = \frac{q_5q_2q_6 - q_3^2q_4^2}{\sqrt{\frac{m_{g_{nr}}}{\Omega_{g_{nr}}}}q_1q_3\sqrt{\frac{m_{g_{rf}}}{\Omega_{g_{rf}}}}q_2q_4}, \tag{4.20}$$

where $q_1 = \Gamma(m_{g_{nr}})$, $q_2 = \Gamma(m_{g_{rf}})$, $q_3 = \Gamma(m_{g_{nr}} + \frac{1}{2})$, $q_4 = \Gamma(m_{g_{rf}} + \frac{1}{2})$, $q_5 = \Gamma(m_{g_{nr}} + 1)$, and $q_6 = \Gamma(m_{g_{rf}} + 1)$. Hence, the expression in (4.15) can be obtained by substituting (4.18) into (4.16).

This concludes the proof of Lemma 4. ■

4.1.3 Ergodic Rate

In FTS, the ergodic rates of NU and FU are, respectively, defined as

$$R_n = \mathbb{E}\left[\log_2\left(1 + SNR_n\right)\right] \text{ and} \tag{4.21}$$

$$R_{f1} = \mathbb{E}\left[\log_2\left(1 + SINR_{f1}\right)\right]. \tag{4.22}$$

In STS, the ergodic rate of FU can be defined as

$$R_{f2} = \mathbb{E}\left[\log_2\left(1 + SNR_{f2}\right)\right]. \tag{4.23}$$

Lemma 5. *The closed-form ergodic rate expression for NU in FTS can be given as in* (3.24).

Proof. The proof can be viewed in Appendix A.2. ■

Lemma 6. *The closed-form ergodic rate expression for FU in FTS and STS can be given, respectively, as in* (3.25) *and* (3.26).

Proof. The proof can be viewed in Appendix A.3. ■

$$R_n = \left[\frac{\pi\, csc\left(\frac{\alpha\pi}{2}\right) {}_1F_2\left(\frac{\alpha}{2}; \frac{1}{2}, 1+\frac{\alpha}{2}; -\frac{\beta^2}{4t}\right)}{\alpha\, t^{\frac{\alpha}{2}}} + \frac{\Gamma(\alpha-2)\, {}_2F_3\left(1,1;2, \frac{3-\alpha}{2}, 2-\frac{\alpha}{2}; -\frac{\beta^2}{4t}\right)}{\beta^{(\alpha-2)}\, t} \right.$$
$$- \frac{\left(2-\alpha-2\alpha^2-\alpha^3\right)\Gamma(\alpha-2)\left(\ln\left(\frac{\beta^2}{t}\right) - 2\phi^{(0)}(\alpha)\right)}{\beta^{\alpha}\ (\alpha+1)}$$
$$\left. - \frac{\beta\pi\, sec\left(\frac{\alpha\pi}{2} {}_1F_2\left(\frac{\alpha+1}{2}; \frac{3}{2}, \frac{\alpha+3}{2}; -\frac{\beta^2}{4t}\right)\right)}{t^{\frac{(\alpha+1)}{2}}\ (\alpha+1)} \right] \frac{\beta^{\alpha}}{\ln(2)\,\Gamma(\alpha)} \tag{3.24}$$

$$R_{f1} = \left[\left(\frac{{}_2F_3\left(1,1;2,1-\frac{a_1}{2}, \frac{3-a_1}{2}; -\frac{1}{4b_1^2 c_1 \gamma_t}\right)}{c_1\, \gamma_t} - \frac{{}_2F_3\left(1,1;2,1-\frac{a_1}{2}, \frac{3-a_1}{2}; -\frac{1}{4b_1^2 c_2 \gamma_t}\right)}{c_2\, \gamma_t} \right) \right.$$
$$\times \frac{\Gamma(a_1-1)}{b_1^2} + \frac{\pi\, csc\left(\frac{\pi a_1}{2}\right)}{b_1^{(a_1+2)}\,(a_1+2)} \left(\frac{{}_1F_2\left(\frac{a_1+1}{2}; \frac{1}{2}, \frac{a_1+3}{2}; -\frac{1}{4b_1^2 c_1 \gamma_t}\right)}{(c_1\, \gamma_t)^{\left(\frac{a_1}{2}+1\right)}} \right.$$
$$\left. - \frac{{}_1F_2\left(\frac{a_1+1}{2}; \frac{1}{2}, \frac{a_1+3}{2}; -\frac{1}{4b_1^2 c_2 \gamma_t}\right)}{(c_2\, \gamma_t)^{\left(\frac{a_1}{2}+1\right)}} \right) + \frac{\pi\, sec\left(\frac{\pi a_1}{2}\right)}{b_1^{(a_1+1)}\,(a_1+1)} \left(\frac{{}_1F_2\left(\frac{a_1+1}{2}; \frac{1}{2}, \frac{a_1+3}{2}; -\frac{1}{4b_1^2 c_1 \gamma_t}\right)}{(c_1\, \gamma_t)^{\left(\frac{a_1+1}{2}\right)}} \right.$$
$$\left. \left. - \frac{{}_1F_2\left(\frac{a_1+1}{2}; \frac{1}{2}, \frac{a_1+3}{2}; -\frac{1}{4b_1^2 c_2 \gamma_t}\right)}{(c_2\, \gamma_t)^{\left(\frac{a_1+1}{2}\right)}} \right) - a\,(a-1)\,\Gamma(a-1) \ln\left(\frac{c_2}{c_1}\right) \right] \frac{1}{\ln(2)\,\Gamma(a_1+1)} \tag{3.25}$$

$$R_{f2} = \frac{1}{\ln(2)\,\Gamma(a_2+1)} \left[\frac{\Gamma(a_2-1)\, {}_2F_3\left(1,1;2,1-\frac{a_2}{2}, \frac{3-a_2}{2}; -\frac{1}{4b_2^2 \gamma_n}\right)}{b_2^2 \gamma_n} - 2a_2\Gamma(a_2-1) \right.$$
$$\times \left(a_2\, \ln\left(\frac{b_2^{-1}}{\sqrt{\gamma_n}}\right) - \ln\left(\frac{b_2^{-1}}{\sqrt{\gamma_n}}\right) - (a_2-1)\ \phi^{(0)}(a_2+1) \right)$$
$$\left. + \frac{csc\left(\frac{\pi a_2}{2}\right) {}_1F_2\left(\frac{a_2}{2}+1; \frac{3}{2}, \frac{a}{2}+2; -\frac{1}{4b_2^2 \gamma_n}\right)}{\pi^{-1}\, b_2^{(a_2+1)}\, \gamma_n^{\frac{(a_2+1)}{2}}\ (a_2+2)} + \frac{sec\left(\frac{\pi a_2}{2}\right) {}_1F_2\left(\frac{a_2+1}{2}; \frac{1}{2}, \frac{a_2+3}{2}; -\frac{1}{4b_2^2 \gamma_n}\right)}{\pi^{-1}\, b_2^{(a+1)}\, \gamma_n^{\frac{(a+1)}{2}}\ (a_2+1)} \right] \tag{3.26}$$

4.1.4 Spectral and Energy Efficiency

SE can be defined as the sum of each rate, as shown below

$$SE = R_n + R_{f1} + R_{f2}. \tag{4.27}$$

To find EE, we can divide SE by the total consumed power, P_{tot}, that is constituted from the total transmitted power and the power consumed by the circuitry within the considered communication system, as follows

$$EE = \frac{SE}{P_{\text{tot}}} = \frac{SE}{(1+\delta)P_t + MP_E + 2P_U + (1+\delta)P_n}, \tag{4.28}$$

where $(1+\delta)\ P_t$, P_E, $(1+\delta)\ P_n$ and P_U denote the dynamic power consumption at BS, power consumed per STAR-RIS element, dynamic power consumption at NU, and the power consumed per user device, respectively [50].

4.2 Simulation Results and Discussions

To comparatively analyse the performance of the designed STAR-RIS-aided CNOMA system, the results also include equivalent NOMA and OMA systems, where OMA employs the TS protocol at STAR-RIS for time division multiplexing. Unless otherwise stated, the system parameters are as listed in Table 4.2. All simulations were done in MATLAB and results were averaged over at least 1000 independent runs.

Table 4.2: Simulation Parameters

Parameter	Value
Power allocation coefficients	$\{\alpha_n^2, \alpha_n^2\} = \{0.3, 0.7\}$ [51, 25]
Shape parameters of fading channels	$\left\{m_{g_{sn}}, m_{g_{sr}}, m_{g_{rn}}, m_{g_{rf}}, m_{h_{nr}}, m_{h_{rf}}\right\} = \{2,5,2,3,2,3\}$ [51]
Spread parameters of fading channels	$\left\{\Omega_{g_{sn}}, \Omega_{g_{sr}}, \Omega_{g_{rn}}, \Omega_{g_{rf}}, \Omega_{h_{nr}}, \Omega_{h_{rf}}\right\} = \{1,1,1,1,1,1\}$
Distance parameters, m	$\left\{d_{sn}, d_{sr}, d_{rn}, d_{rf}\right\} = \{45,50,15,10\}$ [21, 52, 25]
Target rate, bps	$\left\{R_n^{th}, R_f^{th}\right\} = \{5, 1.7\}$ [38]
Ratio of reflecting and transmitting elements	$M_r : M_t = 1:1$
Time-slot allocation coefficients	$\{t_1, t_2\} = \{0.5, 0.5\}$
Noise variance, dBm	$\sigma^2 = -120$ [50]
Transmit power at NU	$P_n = P_t$

Fig. 4.1 displays the OP of NU and FU as the number of STAR-RIS elements increases. The dashed black and magenta curves correspond to NU in NOMA (or FTS) and OMA, respectively, while the solid blue, dashed red and solid black curves are associated with FU in FTS (NOMA), STS and OMA, respectively. General trend is that OP decreases for all users as the number of elements M increases. However, this effect is more noticeable in NOMA and CNOMA only when the signal is transmitted at sufficient power. For instance, at a transmit power of -10

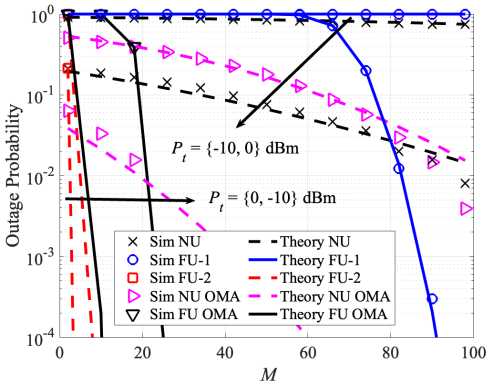

Figure 4.1: OP vs M for different values P_t

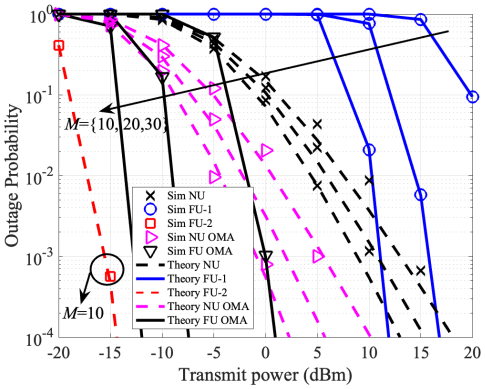

Figure 4.2: OP vs P_t for different values of M

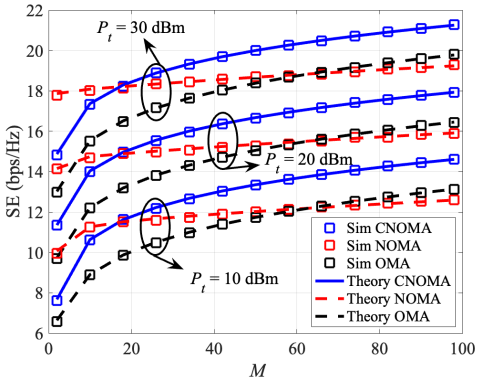

Figure 4.3: SE vs M for different values P_t

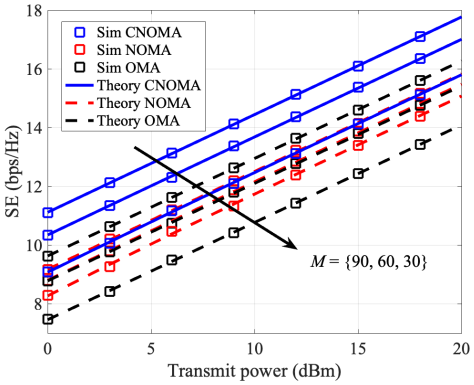

Figure 4.4: SE vs P_t for different values of M

dBm, the OP curves for FTS change slowly compared to those at 0 dBm. However, the OP for FU follows a steep curve, highlighting the impact of interference-free cooperative links. In FTS curves at 0 dBm, although NU initially performs better and its performance remains relatively stable as M increases, FU starts to outperform NU after $M = 80$ for the rest of considered M values. Additionally, it's worth noting that OMA performs better than NOMA. This is because the TS protocol efficiently uses all resources of the STAR-RIS to help each user, and also because received OMA signals are free from interference. Similarly, FU's outage probability is significantly reduced in STS compared to FTS. This is mainly due to the interference-free connection with a larger number of reflecting elements.

Fig. 4.1 illustrates OP against the transmit power. It is seen that the OP performance improves as the transmit power increases. If to look at how the number of STAR-RIS elements affects performance at different power levels, one can find that the worst performance occurs when $M = 10$, and increasing the number of elements improves the outage performance. For example, in FTS, achieving OP of

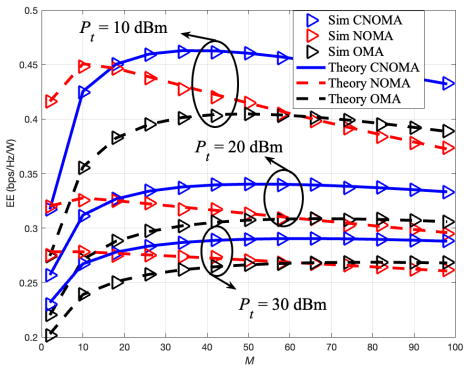

Figure 4.5: EE vs M for different values P_t

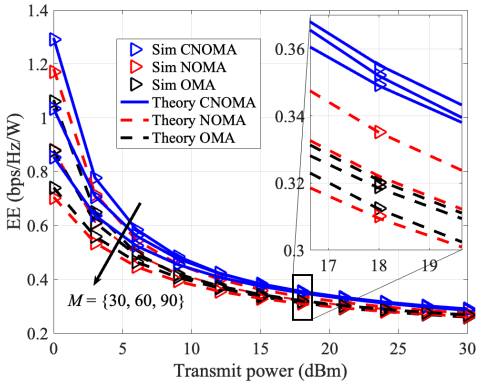

Figure 4.6: EE vs P_t for different values of M

order 10^{-3} requires transmit powers of 16 dBm and 11 dBm when there are 20 and 30 elements, respectively. Furthermore, it can be conluded that the derived theoretical OP expressions match the simulation. However, there's a slight discrepancy between the theoretical and simulated points for NU. This could be due to the approximation of NU's PDF and CDF by the Gamma moment-matching technique, since the derived OP expressions are essentially described through CDF.

Fig. 4.3 depicts SE as the number of STAR-RIS elements varies for different transmit power levels, where the blue, red and black lines correspond to CNOMA, NOMA and OMA, respectively. The plot indicates that SE consistently improves with more STAR-RIS elements. It's important to highlight that there's a specific value of M where CNOMA and OMA surpass NOMA for all considered transmit power levels, which are 18 and 58, respectively. This occurs because NOMA reaches a saturation point faster as the number of STAR-RIS elements increases.

In Fig. 4.4, the system's SE in relation to the transmit power is examined. It's clear that SE increases as transmit power increases. Additionally, CNOMA achieves higher SE than NOMA and OMA for the same number of reflecting elements. For instance, to achieve the same performance as NOMA at 15 dBm transmit power with $M = 90$, CNOMA only needs $M = 30$ at the same transmit power, or it can maintain $M = 90$ and reduce transmit power to 9 dBm. Moreover, under the considered simulation parameters, OMA outperforms non-cooperative NOMA with $M = 90$, despite NOMA usually having an advantage over OMA. This could be because the TS protocol in OMA utilizes twice as many STAR-RIS elements per usage compared to the MS protocol in NOMA.

Fig. 4.5 depicts the EE of the system as the number of STAR-RIS elements varies. It's evident that each curve reaches a peak and then gradually declines after reaching a certain value of M. CNOMA and OMA are more dependent on M than NOMA, resulting in significantly worse performances for CNOMA and OMA when M is low. However, for higher values of M, NOMA experiences a sharper

decline in performance. As the transmit power increases, the performance gap between CNOMA, NOMA, and OMA diminishes. This underscores the importance of determining the optimal number of STAR-RIS elements to prevent resource misuse when considering EE. Additionally, by comparing curves at different transmit power levels, we can infer that the impact of increasing M diminishes at higher transmit power levels. This underscores the complex relationship between the number of STAR-RIS elements and transmit power.

Fig. 4.6 displays the EE of the system in relation to the transmit power. The EE of the system consistently decreases as the transmit power increases. Within the considered range of transmit power levels, CNOMA consistently outperforms NOMA and OMA. However, the performance advantage is most noticeable at lower transmit power values. It's important to note that when transmit power is relatively high, dynamic power consumption outweighs static power consumption according to the total power consumption model described in equation (4.28). Additionally, the gain in SE is linear with the transmit power in dB indicating that SE grows at logarithmic pace with the linear measure of transmit power. This ultimately leads to EE converging to a very low value at high power levels, indicating the limitations of EE improvement under these conditions. Besides, the theoretical results for both SE and EE match the simulations.

Chapter 5

Conclusion

5.1 Accomplished Work

In this study, the performance of the STAR-RIS-aided CNOMA downlink communication system over Nakagami-*m* fading channels was investigated. Specifically, the expressions of OP, SE, and EE were derived in the closed form, the correctness of which was validated through Monte-Carlo simulations. From the simulation results, it is evident that the performance of NOMA can be further enhanced by introducing an interference-free cooperative link between paired users when a sufficient number of the STAR-RIS elements is utilized. Additionally, it was found that the proposed system demonstrates diverse behavior for different sets of parameters. Hence, highlighting the dynamic nature of the system's performance and the interplay between the number of the STAR-RIS elements and transmit power levels that could be used to leverage accessible resources.

5.2 Future Work

A more comprehensive understanding of the performance boundaries of the proposed system model and a more fair comparison with other benchmark scenarios can be achieved by taking into consideration the joint clustering and optimization of timeslots' duration, power allocation coefficients, and the ratio of reflecting and transmitting elements. Furthermore, the system model can be improved through the consideration of hardware impairments such as imperfect SIC, discrete RIS phase-shifts, etc. Which will be the subject of a subsequent work.

Bibliography

[1] Walid Saad, Mehdi Bennis, and Mingzhe Chen. "A Vision of 6G Wireless Systems: Applications, Trends, Technologies, and Open Research Problems". In: *IEEE Network* 34.3 (2020), pp. 134–142. DOI: 10.1109/MNET.001.1900287.

[2] Wei Jiang et al. "The Road Towards 6G: A Comprehensive Survey". In: *IEEE Open Journal of the Communications Society* 2 (2021), pp. 334–366. DOI: 10.1109/OJCOMS.2021.3057679.

[3] Marco Di Renzo et al. "Smart radio environments empowered by reconfigurable AI meta-surfaces: An idea whose time has come". In: *EURASIP Journal on Wireless Communications and Networking* 2019.1 (2019), pp. 1–20. DOI: 10.1186/s13638-019-1438-9.

[4] Zhandos Zhakipov et al. "Accurate Approximation to Channel Distributions of Cascaded RIS-Aided Systems With Phase Errors Over Nakagami-m Channels". In: *IEEE Wireless Communications Letters* 12.5 (2023), pp. 922–926. DOI: 10.1109/LWC.2023.3251647.

[5] Sultangali Arzykulov et al. "Artificial Noise and RIS-Aided Physical Layer Security: Optimal RIS Partitioning and Power Control". In: *IEEE Wireless Communications Letters* (2023), 1–5, DOI: 10.1109/LWC.2023.3256001. DOI: 10.1109/LWC.2023.3256001.

[6] Sultangali Arzykulov et al. "RIS-Assisted Full-Duplex Relay Systems". In: *IEEE Systems Journal* 16.4 (2022), pp. 5729–5740. DOI: 10.1109/JSYST.2022.3189850.

[7] Qingqing Wu et al. "Intelligent Reflecting Surface-Aided Wireless Communications: A Tutorial". In: *IEEE Transactions on Communications* 69.5 (2021), pp. 3313–3351. DOI: 10.1109/TCOMM.2021.3051897.

[8] Mohd Hamza Naim Shaikh et al. "Performance of RIS-empowered NOMA-based D2D Communication under Nakagami-*m* Fading". In: *IEEE 96th Vehicular Technology Conference (VTC2022-Fall)*. 2022, pp. 1–5. DOI: 10.1109/VTC2022-Fall57202.2022.10012767.

[9] Yuanwei Liu et al. “STAR: Simultaneous Transmission and Reflection for 360° Coverage by Intelligent Surfaces”. In: *IEEE Wireless Communications* 28.6 (2021), pp. 102–109. DOI: 10.1109/MWC.001.2100191.

[10] Yuanwei Liu et al. “STAR: Simultaneous Transmission and Reflection for 360° Coverage by Intelligent Surfaces”. In: *IEEE Wireless Communications* 28.6 (2021), pp. 102–109. DOI: 10.1109/MWC.001.2100191.

[11] Refik Caglar Kizilirmak and Hossein Khaleghi Bizaki. “Non-Orthogonal Multiple Access (NOMA) for 5G Networks”. In: *Towards 5G Wireless Networks-A Physical Layer Perspective* 83 (2016), pp. 83–98.

[12] Mingxing Wang et al. “On the Achievable Capacity of Cooperative NOMA Networks: RIS or Relay?” In: *IEEE Wireless Communications Letters* 11.8 (2022), pp. 1624–1628. DOI: 10.1109/LWC.2022.3169806.

[13] Jinliang Huang et al. “On the Achievable Capacity of RIS-NOMA Networks: A Perspective on Elements Number”. In: *Physical Communication* 58 (2023), p. 102045. ISSN: 1874-4907. DOI: https://doi.org/10.1016/j.phycom.2023.102045. URL: https://www.sciencedirect.com/science/article/pii/S1874490723000484.

[14] Beixiong Zheng, Qingqing Wu, and Rui Zhang. “Intelligent Reflecting Surface-Assisted Multiple Access With User Pairing: NOMA or OMA?” In: *IEEE Communications Letters* 24.4 (2020), pp. 753–757. DOI: 10.1109/LCOMM.2020.2969870.

[15] Mohd Hamza Naim Shaikh et al. “On the Performance of RIS-Aided NOMA System with Non-ideal Transceiver over Nakagami-m Fading”. In: *2022 IEEE Wireless Communications and Networking Conference (WCNC)*. 2022, pp. 1737–1742. DOI: 10.1109/WCNC51071.2022.9771831.

[16] Zhandos Zhakipov and Galymzhan Nauryzbayev. “Channel Modeling and Outage Performance of Cascaded RIS-empowered Wireless Networks”. In: *2022 13th International Conference on Information and Communication Technology Convergence (ICTC)*. 2022, pp. 187–192. DOI: 10.1109/ICTC55196.2022.9952786.

[17] Sultangali Arzykulov et al. “RIS-Assisted Full-Duplex Relay Systems”. In: *IEEE Systems Journal* 16.4 (2022), pp. 5729–5740. DOI: 10.1109/JSYST.2022.3189850.

[18] Chongwen Huang et al. “Reconfigurable Intelligent Surfaces for Energy Efficiency in Wireless Communication”. In: *IEEE Transactions on Wireless Communications* 18.8 (2019), pp. 4157–4170. DOI: 10.1109/TWC.2019.2922609.

[19] Qingqing Wu and Rui Zhang. "Intelligent Reflecting Surface Enhanced Wireless Network via Joint Active and Passive Beamforming". In: *IEEE Transactions on Wireless Communications* 18.11 (2019), pp. 5394–5409. DOI: 10.1109/TWC.2019.2936025.

[20] Xidong Mu et al. "Exploiting Intelligent Reflecting Surfaces in NOMA Networks: Joint Beamforming Optimization". In: *IEEE Transactions on Wireless Communications* 19.10 (2020), pp. 6884–6898. DOI: 10.1109/TWC.2020.3006915.

[21] Xidong Mu et al. "Simultaneously Transmitting and Reflecting (STAR) RIS Aided Wireless Communications". In: *IEEE Transactions on Wireless Communications* 21.5 (2022), pp. 3083–3098. DOI: 10.1109/TWC.2021.3118225.

[22] Fang Fang et al. "Energy-Efficient Design of STAR-RIS Aided MIMO-NOMA Networks". In: *IEEE Transactions on Communications* 71.1 (2023), pp. 498–511. DOI: 10.1109/TCOMM.2022.3223706.

[23] Haochun Ma et al. "Transmit Power Minimization for STAR-RIS-Empowered Uplink NOMA System". In: *IEEE Wireless Communications Letters* 11.11 (2022), pp. 2430–2434. DOI: 10.1109/LWC.2022.3205703.

[24] Dulaj Gunasinghe, Dhanushka Kudathanthirige, and Gayan Amarasuriya Aruma Baduge. "The Achievable Rate Performance of STAR-RIS Aided Massive MIMO Systems". In: *IEEE Transactions on Communications* (2024), pp. 1–1. DOI: 10.1109/TCOMM.2024.3361549.

[25] Dulaj Gunasinghe and Gayan Amarasuriya. "Performance Analysis of STAR-RIS for Wireless Communication". In: *ICC 2022 - IEEE International Conference on Communications*. 2022, pp. 3275–3280. DOI: 10.1109/ICC45855.2022.9838939.

[26] Xinwei Yue et al. "Simultaneously Transmitting and Reflecting Reconfigurable Intelligent Surface Assisted NOMA Networks". In: *IEEE Transactions on Wireless Communications* 22.1 (2023), pp. 189–204. DOI: 10.1109/TWC.2022.3192211.

[27] Jiagao Chen and Xiangbin Yu. "Ergodic Rate Analysis and Phase Design of STAR-RIS Aided NOMA With Statistical CSI". In: *IEEE Communications Letters* 26.12 (2022), pp. 2889–2893. DOI: 10.1109/LCOMM.2022.3202346.

[28] Xingwang Li et al. "Performance Analysis of STAR-RIS-CR-NOMA Based Consumer IoT Networks for Resilient Industry 5.0". In: *IEEE Transactions on Consumer Electronics* (2023), pp. 1–1. DOI: 10.1109/TCE.2023.3319402.

[29] Lei Wang et al. "Joint Reliability Optimization and Beamforming Design for STAR-RIS-Aided Multi-user MISO URLLC systems". In: *IEEE Transactions on Vehicular Technology* (2024), pp. 1–15. DOI: 10.1109/TVT.2024.3349509.

[30] Yasoub Eghbali et al. “Providing URLLC Service in Multi-STAR-RIS Assisted and Full-Duplex Cellular Wireless Systems: A Meta-Learning Approach”. In: *IEEE Communications Letters* (2024), pp. 1–1. DOI: 10.1109/LCOMM.2023.3349377.

[31] Chenyu Wu et al. “Resource Allocation in STAR-RIS-Aided Networks: OMA and NOMA”. In: *IEEE Transactions on Wireless Communications* 21.9 (2022), pp. 7653–7667. DOI: 10.1109/TWC.2022.3160151.

[32] Jiaqi Xu, Yuanwei Liu, and Xidong Mu. “Performance Analysis for the Coupled Phase-Shift STAR-RISs”. In: *2022 IEEE Wireless Communications and Networking Conference (WCNC)*. 2022, pp. 489–493. DOI: 10.1109/WCNC51071.2022.9771900.

[33] Jiaqi Xu et al. “STAR-RISs: A Correlated T&R Phase-Shift Model and Practical Phase-Shift Configuration Strategies”. In: *IEEE Journal of Selected Topics in Signal Processing* 16.5 (2022), pp. 1097–1111. DOI: 10.1109/JSTSP.2022.3175030.

[34] Na Xue et al. “NOMA Assisted Full Space STAR-RIS-ISAC”. In: *IEEE Transactions on Wireless Communications* (2024), pp. 1–1. DOI: 10.1109/TWC.2024.3357349.

[35] Farjam Karim et al. “STAR-RIS aided Full Duplex Communication System: Performance Analysis”. In: *GLOBECOM 2022 - 2022 IEEE Global Communications Conference*. 2022, pp. 3114–3119. DOI: 10.1109/GLOBECOM48099.2022.10001603.

[36] Jiaqi Xu et al. “Simultaneously Transmitting and Reflecting (STAR)-RISs: Are They Applicable to Dual-Sided Incidence?” In: *IEEE Wireless Communications Letters* 12.1 (2023), pp. 129–133. DOI: 10.1109/LWC.2022.3219017.

[37] Jiguang He, Aymen Fakhreddine, and George C. Alexandropoulos. “Simultaneous Indoor and Outdoor 3D Localization with STAR-RIS-Assisted Millimeter Wave Systems”. In: *2022 IEEE 96th Vehicular Technology Conference (VTC2022-Fall)*. 2022, pp. 1–6. DOI: 10.1109/VTC2022-Fall57202.2022.10013055.

[38] Jerry Chun-Wei Lin Hsing-Chung Chen Agung Mulyo Widodo and Chien-Erh. Weng. “Reconfigurable Intelligent Surface-Aided Cooperative NOMA with p-CSI Fading Channel toward 6G-Based IoT System”. In: *Sensors* 22.19 (2022). DOI: 10.3390/s22197664.

[39] Jinyong Sun Xiang Zhao. “Performance Analysis of Reconfigurable Intelligent Surface-Aided Full-Duplex Cooperative NOMA System”. In: *Wireless Communications and Mobile Computing* (2021). DOI: 10.1155/2021/5550235.

[40] Juanjuan Ren et al. “RIS-Assisted Cooperative NOMA With SWIPT”. In: *IEEE Wireless Communications Letters* 12.3 (2023), pp. 446–450. DOI: 10.1109/LWC.2022.3229843.

[41] Guoan Zhang et al. “Hybrid Time-Switching and Power-Splitting EH Relaying for RIS-NOMA Downlink”. In: *IEEE Transactions on Cognitive Communications and Networking* 9.1 (2023), pp. 146–158. DOI: 10.1109/TCCN.2022.3216406.

[42] Khac-Tuan Nguyen, Thai-Hoc Vu, and Sunghwan Kim. “A Unified Framework Analysis for Reconfigurable Intelligent Surface-Aided Coordinated NOMA Systems”. In: *IEEE Transactions on Vehicular Technology* (2023), pp. 1–6. DOI: 10.1109/TVT.2023.3285629.

[43] Sun Mao et al. “Intelligent Reflecting Surface Enhanced D2D Cooperative Computing”. In: *IEEE Wireless Communications Letters* 10.7 (2021), pp. 1419–1423. DOI: 10.1109/LWC.2021.3069095.

[44] Yongming Huang et al. “Signal Processing for MIMO-NOMA: Present and Future Challenges”. In: *IEEE Wireless Communications* 25.2 (2018), pp. 32–38. DOI: 10.1109/MWC.2018.1700108.

[45] Yanyu Cheng et al. “Downlink and Uplink Intelligent Reflecting Surface Aided Networks: NOMA and OMA”. In: *IEEE Transactions on Wireless Communications* (2021), pp. 1–1. DOI: 10.1109/TWC.2021.3054841.

[46] Emil Bjornson, Ozgecan Ozdogan, and Erik G Larsson. “Intelligent reflecting surface versus decode-and-forward: How large surfaces are needed to beat relaying?” In: *IEEE Wirel. Commun. Lett.* 9.2 (2019), pp. 244–248.

[47] Minchae Jung et al. “Reliability Analysis of Large Intelligent Surfaces (LISs): Rate Distribution and Outage Probability”. In: *IEEE Wireless Communications Letters* 8.6 (2019), pp. 1662–1666. DOI: 10.1109/LWC.2019.2935190.

[48] Sandrine Boumard et al. “Comparison of Spectral and Energy Efficiency Metrics Using Measurements in a LTE-A Network”. In: *2018 Network Traffic Measurement and Analysis Conference (TMA)*. 2018, pp. 1–8. DOI: 10.23919/TMA.2018.8506529.

[49] Mohd Hamza Naim Shaikh et al. “Performance Analysis of Intelligent Reflecting Surface-Assisted Wireless System With Non-Ideal Transceiver”. In: *IEEE Open J. Commun. Soc.* 2 (2021), pp. 671–686. DOI: 10.1109/OJCOMS.2021.3068866.

[50] Mohd Hamza Naim Shaikh et al. “A Downlink RIS-Aided NOMA System With Hardware Impairments: Performance Characterization and Analysis”. In: *IEEE Open Journal of Signal Processing* 3 (2022), pp. 288–305. DOI: 10.1109/OJSP.2022.3194416.

[51] Boqun Zhao et al. "Ergodic Rate Analysis of STAR-RIS Aided NOMA Systems". In: *IEEE Communications Letters* 26.10 (2022), pp. 2297–2301. DOI: 10.1109/LCOMM.2022.3194363.

[52] Jiagao Chen and Xiangbin Yu. "Ergodic Rate Analysis and Phase Design of STAR-RIS Aided NOMA With Statistical CSI". In: *IEEE Communications Letters* 26.12 (2022), pp. 2889–2893. DOI: 10.1109/LCOMM.2022.3202346.

Appendix A

Appendix A

A.1 Proof of Lemma 1

For the proof it is enough to evaluate $\mathbb{E}[|\mathcal{G}_n|]$ and $\mathbb{V}[|\mathcal{G}_n|]$ as the resulting expressions can be directly substituted to estimate α and β parameters of the Gamma distribution.

Finding $\mathbb{E}[|\mathcal{G}_n|]$:

$$\begin{aligned}\mathbb{E}\left[|\mathcal{G}_n|\right] &= \mathbb{E}\left[\sqrt{\Lambda_{sn}}\,|g_{sn}| + \sqrt{\Lambda_{sr}\,\Lambda_{rn}}\sum_{i=1}^{M_r}\left|g_{sr}^{(i)}\right|\,\left|g_{rn}^{(i)}\right|\right],\\ &= \sqrt{\Lambda_{sn}}\,\mathbb{E}\left[|g_{sn}|\right] + \sqrt{\Lambda_{sr}\,\Lambda_{rn}}\sum_{i=1}^{M_r}\mathbb{E}\left[\left|g_{sr}^{(i)}\right|\right]\,\mathbb{E}\left[\left|g_{rn}^{(i)}\right|\right]. \qquad \text{(A.1.1)}\end{aligned}$$

Furthermore, since all random variables (RVs) on the right-hand side of (A.1.1) are Nakagami-m distributed, it can be further defined as

$$\begin{aligned}\mathbb{E}[|\mathcal{G}_n|] &= \sqrt{\Lambda_{sr}\,\Lambda_{rn}}\,M_r\,\frac{\Gamma(m_{g_{sr}}+\frac{1}{2})\Gamma(m_{g_{rn}}+\frac{1}{2})}{\Gamma(m_{g_{sr}})\Gamma(m_{g_{rn}})}\\ &\times\sqrt{\frac{\Omega_{g_{sr}}\Omega_{g_{rn}}}{m_{g_{sr}}m_{g_{rn}}}} + \sqrt{\Lambda_{sn}}\,\frac{\Gamma(m_{g_{sn}}+\frac{1}{2})}{\Gamma(m_{g_{sn}})}\sqrt{\frac{\Omega_{g_{sn}}}{m_{g_{sn}}}}. \qquad \text{(A.1.2)}\end{aligned}$$

Finding $\mathbb{V}[|\mathcal{G}_n|]$:

$$\mathbb{V}[|\mathcal{G}_n|] = \mathbb{V}\left[\sqrt{\Lambda_{sn}}\,|g_{sn}| + \sqrt{\Lambda_{sr}\,\Lambda_{rn}}\sum_{i=1}^{M_r}\left|g_{sr}^{(i)}\right|\,\left|g_{rn}^{(i)}\right|\right]. \qquad \text{(A.1.3)}$$

Since all members of the summation are uncorrelated RVs, the expression in (A.1.3) can be re-written as

$$\mathbb{V}[|\mathcal{G}_n|] = \Lambda_{sn}\,\mathbb{V}\left[|g_{sn}|\right] + \Lambda_{sr}\,\Lambda_{rn}\sum_{i=1}^{M_r}\underbrace{\mathbb{V}\left[\left|g_{sr}^{(i)}\right|\,\left|g_{rn}^{(i)}\right|\right]}_{\mathcal{I}}, \qquad \text{(A.1.4)}$$

where $\mathcal{I}$ can be defined as

$$\begin{aligned}\mathcal{I} &= \mathbb{E}\left[\left|g_{sr}^{(i)}\right|^2\right]\mathbb{E}\left[\left|g_{rn}^{(i)}\right|^2\right] - \mathbb{E}\left[\left|g_{sr}^{(i)}\right|\right]^2\mathbb{E}\left[\left|g_{rn}^{(i)}\right|\right]^2 \\ &= \Omega_{g_{sr}}\Omega_{g_{rn}} - \left(\frac{\Gamma(m_{g_{sr}}+\frac{1}{2})\Gamma(m_{g_{rn}}+\frac{1}{2})}{\Gamma(m_{g_{sr}})\Gamma(m_{g_{rn}})}\right)^2 \frac{\Omega_{g_{sr}}\Omega_{g_{rn}}}{m_{g_{sr}}m_{g_{rn}}} \end{aligned} \tag{A.1.5}$$

Substituting this into (A.1.4) yields the following

$$\begin{aligned}\mathbb{V}[|\mathcal{G}_n|] = \Lambda_{sn}\,\Omega_{g_{sn}} &- \Lambda_{sn}\,\frac{\Omega_{g_{sn}}}{m_{g_{sn}}}\left(\frac{\Gamma(m_{g_{sn}}+\frac{1}{2})}{\Gamma(m_{g_{sn}})}\right)^2 \\ &- \frac{M_r\Omega_{g_{sr}}\Omega_{g_{rn}}}{m_{g_{sr}}m_{g_{rn}}}\left(\frac{\Gamma(m_{g_{sr}}+\frac{1}{2})\Gamma(m_{g_{rn}}+\frac{1}{2})}{\Gamma(m_{g_{sr}})\Gamma(m_{g_{rn}})}\right)^2 \\ &\times \Lambda_{sr}\,\Lambda_{rn} + \Lambda_{sr\,\Lambda_{rn}}\,M_r\Omega_{g_{sr}}\Omega_{g_{rn}}. \end{aligned} \tag{A.1.6}$$

This concludes the proof of Lemma 1.

A.2 Proof of Lemma 4

The ergodic rate of NU, R_n, can be defined from (4.21) as

$$R_n = \mathbb{E}\left[\log_2\left(1 + t\,|\mathcal{G}_n|^2\right)\right], \tag{A.2.1}$$

where $t = \alpha_n^2\,\gamma_t$. Expanding the expression above gives

$$R_n = \int_0^\infty \frac{\ln\left(1+t|\mathcal{G}_n|^2\right)}{\ln(2)} f_{|\mathcal{G}_n|}(x)\mathrm{d}x = \frac{\beta^\alpha}{\ln(2)\Gamma(\alpha)}\int_0^\infty \ln(1+tx^2)x^{(\alpha-1)}e^{-\beta x}\mathrm{d}x \tag{A.2.2}$$

The expression above can be further simplified using the identity $\ln(x+1) = x\,{}_2F_1(1,1;2;-x)$ as follows

$$R_n = \frac{\beta^\alpha t}{\ln(2)\Gamma(\alpha)}\int_0^\infty {}_2F_1(1,1;2;-tx^2)\,x^{(\alpha+1)}e^{-\beta x}\mathrm{d}x, \tag{A.2.3}$$

which can be solved using [**math**] and presented as in (3.24).

This concludes the proof of Lemma 4.

A.3 Proof of Lemma 5

The ergodic rate of FU in FTS, R_{f1}, can be defined from (4.22) as

$$R_{f1} = \mathbb{E}\left[\log_2\left(1 + \frac{|\mathcal{G}_{f1}|^2\,\alpha_f^2\,\gamma_t}{|\mathcal{G}_{f1}|^2\,\alpha_n^2\gamma_t + 1}\right)\right]. \tag{A.3.1}$$

After expanding the expression above and some algebraic manipulations, it can be represented as

$$R_{f1} = \frac{1}{\ln(2)} \left[\underbrace{\int_0^\infty \ln(1 + c_1\, x) f_{|\mathcal{G}_{f1}|^2}(x) \mathrm{d}x}_{\mathcal{K}_1} - \underbrace{\int_0^\infty \ln(1 + c_2\, x) f_{|\mathcal{G}_{f2}|^2}(x) \mathrm{d}x}_{\mathcal{K}_2} \right], \quad \text{(A.3.2)}$$

where $c_1 = (\alpha_n^2 + \alpha_f^2)\gamma_t$ and $c_2 = \alpha_n^2 \gamma_t$.

Like (A.2.3), $\mathcal{K}_1$ and $\mathcal{K}_2$ can be simplified and defined as

$$\mathcal{K}_1 = c_1 \int_0^\infty \frac{x^{\frac{a_1+1}{2}} \exp\left(\frac{-\sqrt{x}}{b_1^2}\right) {}_2F_1(1, 1; 2; -c_1 x)}{2\, b_1^{(a_1+1)} \Gamma(a_1 + 1)} \mathrm{d}x \quad \text{(A.3.3)}$$

$$\mathcal{K}_2 = c_2 \int_0^\infty \frac{x^{\frac{a_1+1}{2}} \exp\left(\frac{-\sqrt{x}}{b_1^2}\right) {}_2F_1(1, 1; 2; -c_2 x)}{2\, b_1^{(a_1+1)} \Gamma(a_1 + 1)} \mathrm{d}x \quad \text{(A.3.4)}$$

Solving the equations above as in [**math**] and substituting them into (A.3.2) gives the expression that can be presented as in (3.25).

The ergodic rate of FU in STS, R_{f2}, can be defined from (4.23) as

$$R_{f2} = \mathbb{E}\left[\log_2\left(1 + |\mathcal{G}_{f2}|^2 \gamma_n\right)\right] = \frac{1}{\ln(2)} \int_0^\infty \ln(1 + \gamma_n\, x) f_{|\mathcal{G}_{f2}|^2}(x) \mathrm{d}x. \quad \text{(A.3.5)}$$

Hence, the expression above can be solved in a similar way $\mathcal{K}_1$ was solved and presented as in (3.26).

This concludes the proof of Lemma 5.